

# Nuclear-order-induced quantum criticality and heavy-fermion superconductivity at ultra-low temperatures in YbRh<sub>2</sub>Si<sub>2</sub>

Erwin Schubert<sup>1</sup>, S. Wirth<sup>2</sup> and Frank Steglich<sup>2,3,\*</sup>

<sup>1</sup>*Physics Department, Technical University of Munich, 80333 Munich, Germany*

<sup>2</sup>*Max-Planck-Institute for Chemical Physics of Solids, Nöthnitzer Str. 40, 01187 Dresden, Germany*

<sup>3</sup>*Center for Correlated Matter, Zhejiang University, Hangzhou, Zhejiang 310058, China*

(Dated: April 28, 2022)

The tetragonal heavy-fermion metal YbRh<sub>2</sub>Si<sub>2</sub> orders antiferromagnetically at  $T_N = 70$  mK and exhibits an unconventional quantum critical point (QCP) of Kondo-destroying type at  $B_N = 60$  mT, for the magnetic field applied within the basal ( $a, b$ ) plane. Ultra-low-temperature magnetization and heat-capacity measurements at very low fields indicate that the  $4f$ -electronic antiferromagnetic (AF) order is strongly suppressed by a nuclear-dominated hybrid order ('A-phase') at  $T_A \leq 2.3$  mK, such that quantum critical fluctuations develop at  $B \approx 0$  [1]. This enables the onset of heavy-fermion superconductivity ( $T_c = 2$  mK) which appears to be suppressed by the primary AF order at elevated temperatures. Measurements of the Meissner effect reveal bulk superconductivity, with  $T_c$  decreasing under applied field to  $T_c < 1$  mK at  $B > 20$  mT. The observation of a weak but distinct superconducting shielding signal at a temperature as high as 10 mK suggests the formation of insulated random islands with emergent A-phase order and superconductivity. Upon cooling, the shielding signal increases almost linearly in temperature, indicating a growth of the islands which eventually percolate at  $T \approx 6.5$  mK. Recent electrical-resistivity results by [2] confirm the existence of superconductivity in YbRh<sub>2</sub>Si<sub>2</sub> at ultra-low temperatures. The combination of the results of [1] and [2] at ultra-low temperatures below  $B_N$ , along with those previously established at higher temperatures in the paramagnetic state, provide compelling evidence that the Kondo-destruction quantum criticality robustly drives unconventional superconductivity.

## I. KONDO-DESTROYING, FIELD-INDUCED QUANTUM CRITICAL POINT

Lanthanide-based intermetallic compounds showing heavy-fermion phenomena are well understood within the framework of the Kondo lattice [3]. The localized open  $4f$ -shells of such materials are characterized by a distinct hierarchy of fundamental energy scales, the local Coulomb repulsion and Hund's rule energies, spin-orbit coupling, crystal-field splitting, Kondo screening including excited crystal-field states at an elevated temperature, where the formation of hybridized  $4f$ -bands starts to be recognized in ARPES measurements [4]), as well as Kondo screening of the lowest-lying crystal-field-derived Kramers doublet ( $k_B T_K$ ). As illustrated below, the single-ion Kondo temperature  $T_K$  was found to be identical to  $T_{\text{coh}}$  [5, 6] where spatial coherence among  $4f$ -shells sets in as seen in transport measurements.

The onsite Kondo screening competes with the inter-site magnetic Ruderman–Kittel–Kasuya–Yosida (RKKY) interaction. While predominant Kondo screening results in a paramagnetic heavy-fermion ground state, a dominant RKKY interaction causes magnetic, most frequently antiferromagnetic (AF), order. For a substantial number of these heavy-fermion metals the Kondo screening turns out to almost exactly cancel the RKKY interaction. In this situation, a continuous transition may exist at  $T = 0$  between the heavy-fermion and the AF phase. This continuous quantum phase transition or quantum critical

point (QCP) can be tuned by a non-thermal control parameter, e.g., pressure or magnetic field [7–10].

YbRh<sub>2</sub>Si<sub>2</sub> is a prototypical heavy-fermion metal [5, 11] which orders antiferromagnetically at a Néel temperature  $T_N = 70$  mK [12]. Because of a strong magnetic anisotropy the critical field  $B_N$  at which AF order smoothly disappears is only 60 mT when the field is applied within the basal tetragonal ( $a, b$ ) plane, i.e., it is more than ten times lower compared to  $B_N \parallel c$  [13]. The staggered moment was shown to be very small,  $\mu_{\text{AF}} \approx 0.002 \mu_B$  [14]. Both the low-temperature paramagnetic ( $B > B_N$ ) and AF phases ( $B < B_N$ ) behave as heavy Fermi liquids [13] whereas a funnel-shaped quantum critical regime in the  $B$ - $T$  phase diagram (Fig. 1) with non-Fermi-liquid properties is centered at the critical field  $B_N$ . The AF phase transition is of second order to the lowest temperature (20 mK) accessible in magnetostriction measurements [15]; the crossover between the paramagnetic Fermi liquid and the non-Fermi-liquid phase turns out to be quite broad. The sub-linear white  $T^*(B)$  crossover line in Fig. 1 was constructed by the midpoints of thermally broadened jumps in both the longitudinal magneto-resistivity and the isothermally measured initial normal Hall coefficient [16, 17]. They agree satisfactorily with the locations of distinct anomalies in the field dependence of both the isothermal DC magnetization and magnetostriction as well as in the temperature dependence of the AC susceptibility measured at fixed magnetic field [15].  $T^*(B)$  indicates a crossover between a small Fermi volume ('small Fermi surface') at low fields and a large one at elevated fields. The crossover width (grey shaded

\* steglich@cpfs.mpg.de

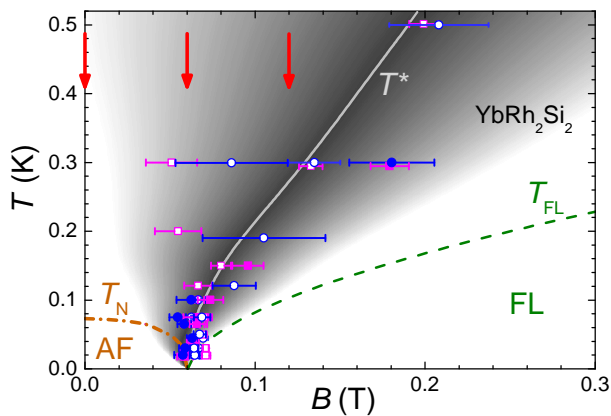


FIG. 1. Temperature–magnetic field phase diagram of  $\text{YbRh}_2\text{Si}_2$  for  $B \perp c$ . The symbols mark the results from Hall and magnetoresistance measurements on two different samples from which the Fermi surface crossover temperature  $T^*$ -line is estimated [17]. The grey scale visualizes the slope of isothermal magnetoresistance. Orange and green dashed lines indicate the Néel temperature  $T_N$  and the crossover temperature  $T_{FL}$  below which AF order and Fermi liquid behavior are observed, respectively. Red arrows indicate  $B = 0, B_N$  and  $2B_N$ , respectively. Figure adapted from [3].

region) turns out to be proportional to  $T$ . The QCP at  $B_N(T = 0)$  is of an unconventional ‘local’ (instead of itinerant) variety, which may be called a ‘partial Mott’ or Kondo-destroying QCP. It is characterized by a dynamical spin susceptibility with frequency-over-temperature scaling and a fractional exponent in the singular parts of both the frequency and temperature dependences [18, 19] as observed by inelastic neutron scattering on both  $\text{UCu}_{5-x}\text{Pd}_x$  [20] and  $\text{CeCu}_{6-x}\text{Au}_x$  [21]. The latter material [22] as well as  $\text{CeRhIn}_5$  [23, 24] are also prototypical heavy-fermion metals exhibiting a local QCP.

Figure 2 displays the thermal evolution at low temperatures of both the (Sommerfeld) coefficient of the  $4f$ -derived part of the specific heat,  $\gamma = C_{el}/T = C_{4f}/T$  (Fig. 2A), and the electrical resistivity measured on an  $\text{YbRh}_2\text{Si}_2$  single crystal with a low residual resistivity of about  $0.5 \mu\Omega\text{cm}$  (Fig. 2B), at  $B = 0, B_N$  and  $2B_N$ , respectively (see red arrows in Fig. 1). The behavior of a heavy Fermi liquid in both the AF and low-temperature paramagnetic phase is clearly resolved by a huge constant  $\gamma$ -value (Fig. 2A) and a pronounced  $T^2$ -dependence in  $\rho(T)$  (Fig. 2B). Very peculiarly, the Fermi liquid in the AF phase (with small Fermi surface as  $T \rightarrow 0$ ) is considerably heavier than the Fermi liquid in the paramagnetic phase (with large Fermi surface). Approaching the QCP at  $B = B_N$  by cooling to below 0.3 K, one finds that  $\gamma(T)$  diverges following a power-law dependence with a critical exponent of  $\approx -0.3$  [25]. As shown in the inset of Fig. 2A,  $\gamma(T)$  obeys a logarithmic  $T$ -dependence [25]

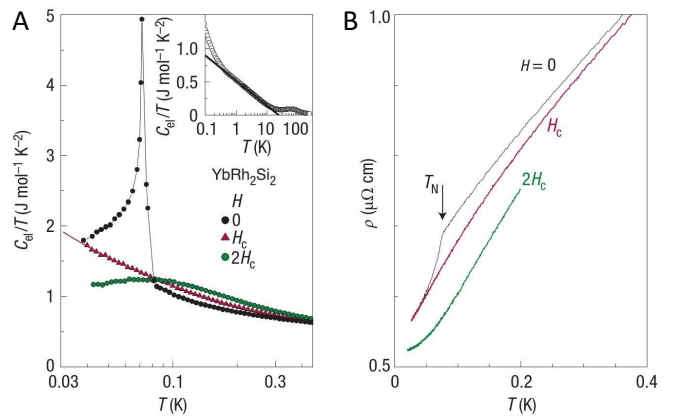


FIG. 2. **(A)** Sommerfeld coefficient of the electronic specific heat and **(B)** electrical resistivity vs. temperature  $T$  at  $B = 0, B_N$  and  $2B_N$  for a  $\text{YbRh}_2\text{Si}_2$  single crystal with  $RRR = 150$ . Inset in A shows the Sommerfeld coefficient at  $B_N = 60$  mT between 0.1 K and room temperature. Reproduced from [9].

at elevated temperature. The incremental resistivity measured at  $B = B_N$  on a very clean single crystal is strictly linear in  $T$ ,  $\Delta\rho(T) = \rho(T) - \rho_0 = A'T$ , at  $T < 0.1$  K. Over a broad temperature range up to  $T = 10$  K, the resistivity semi-quantitatively follows a  $T$ -linear dependence, although the ‘temperature-dependent resistivity exponent’, defined as  $d \ln(\rho - \rho_0)/d \ln T$ , shows some variation that is clustered around 1 [26]. For a single crystal with nominally 5% Ge substituted for Si showing a five times larger residual resistivity,  $\Delta\rho(T) = A'T$  is more strictly observed all the way up to  $T = 10$  K [25], which suggests a degree of disorder modulation to this ‘strange-metal’ behavior. If one restricts to a relatively narrow temperature range,  $\Delta\rho(T)$  has also been fit with other exponents,  $A''T^\alpha$  ( $\alpha < 1$ ); this includes the case of  $\alpha = 3/4$  in the temperature window  $0.4 \text{ K} < T < 1 \text{ K}$  for the high-quality crystal exploited in Fig. 2B, as motivated by the theory of ‘critical quasiparticles’ [27] (which, however, is inapt to explain the measured asymptotic linear-in- $T$  dependence of the resistivity at the unconventional QCP in  $\text{YbRh}_2\text{Si}_2$ ). Most importantly, though, for all samples studied so far, the asymptotic ( $T \rightarrow 0$ )  $T$ -dependence of  $\rho(T)$  registered at  $B = B_N$  is found to be linear, see also [2]. The linear-in- $T$  coefficient,  $A'$ , can be converted to a linear-in- $T$  coefficient in the scattering rate,  $1/\tau$ , in a procedure based on a Drude analysis: the latter is found to be much smaller than what appears in a Planckian form when a ‘background’ heavy-fermion value is used for the effective mass [2, 28].

One of the important techniques that provides new insight into such correlation-driven phenomena is scanning tunneling spectroscopy (STS) with its unique ability to give local, atomically resolved information that relates to the one-particle Green’s function [29]. However, one

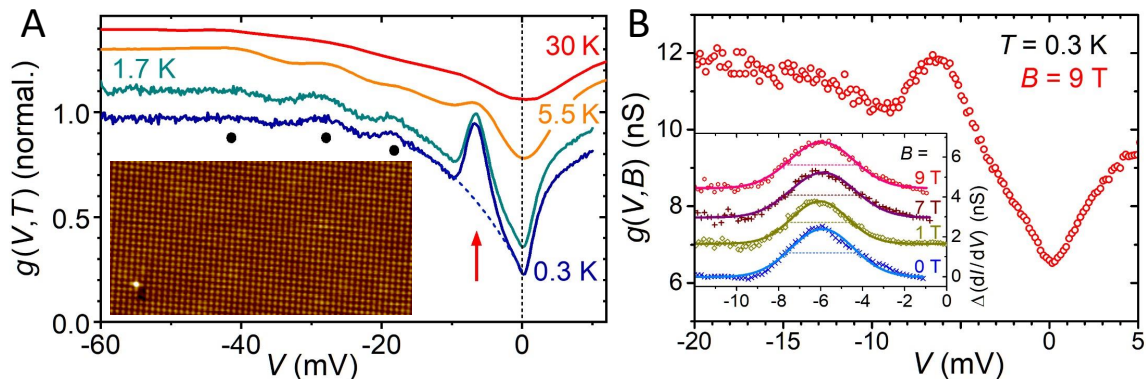


FIG. 3. Tunneling conductance  $g(V, T, B)$  on Si-terminated  $\text{YbRh}_2\text{Si}_2$ . **(A)** Data obtained at different temperatures and  $B = 0$ .  $g(V, T)$ -values are normalized at  $V = -80$  mV and offset for clarity. The  $-6$  meV-peak evolving at low  $T$  is marked by a red arrow; the parabola background for peak analysis at  $T = 0.3$  K is shown as a dashed line. Black dots indicate features resulting from crystalline electric field splitting of the Yb  $4f$  multiplet. Inset: Topography visualizing the excellent surface quality (area:  $20 \times 10$  nm<sup>2</sup>,  $V = 100$  mV,  $I = 0.6$  nA). **(B)** Exemplary in-field data at  $T = 0.3$  K and  $B = 9$  T ( $\parallel c$ ). Inset: Data (markers) after background subtraction with corresponding Gaussian fits (lines). A reduced width (full width at half maximum, dashed lines) of the Gaussian at  $B = 1$  T can be recognized. All figure parts adapted from [6].

of the prerequisites for successful STS measurements is the preparation and perpetuation of clean sample surfaces. Fortunately,  $\text{YbRh}_2\text{Si}_2$  can be cleaved nicely perpendicular to the  $c$ -axis in ultra-high vacuum (UHV) and at low temperatures of about 20 K providing atomically flat surface areas of often several hundreds of nanometers in extent. Such surfaces not only evidence the excellent sample quality (inset to Fig. 3A), they even allow to analyze the defects to be mostly caused by Rh-atoms on Si sites [30].

We here focus on predominantly encountered Si-terminated surfaces. In case of such surfaces, the Kondo-active Yb atoms are located in the fourth-to-topmost layer which prevents a reduced screening of the Yb local moments at the surface [31] and ensures a predominant study of bulk properties by STS. The latter is clearly evidenced by the observation of crystal field excitations in the tunneling spectra [5] at energies in excellent agreement with inelastic neutron scattering data [32] (black dots in Fig. 3A). Moreover, Si-terminated surfaces promote predominant tunneling into the conduction band as compared to the  $4f$  quasiparticle states and thereby simplify the analysis of the obtained spectra as co-tunneling can be neglected [5, 29]. In this simplified picture, the successive formation of the single-ion Kondo effect upon lowering the temperature results primarily in a modification of the density of states of the conduction band seen as a strong decrease of the tunneling conductance  $g(V, T)$  for  $V$  small enough to not break up the quasiparticles. This process is observed to commence at around 100 K and coincides with the onset of local Kondo screening involving excited crystalline electric field levels as concluded from entropy estimates [25]. Upon cooling to below the single-ion Kondo temperature  $T_K \simeq 25$  K the  $4f$  electrons condense into the Kramers doublet ground state and the Kondo

lattice develops. This is reflected in the STS data, Fig. 3A, by the strong development of a peak at around  $-6$  meV. Notably, the position in energy of this peak does not depend on temperature.

The relation of this  $-6$  meV-peak to the Kondo lattice is supported by calculations: Results of a multi-level finite- $U$  non-crossing approximation [5] which does not consider intersite Kondo correlations captures the temperature evolution of the zero-bias conductance dip remarkably well but provides no indication for a peak at  $-6$  meV. Conversely, renormalized band structure calculations [33] which treats the fully renormalized Kondo lattice ground state finds a partially developed hybridization gap at slightly smaller energy in the quasiparticle density of states (which is complementary to the here measured density of states of the conduction band within the Kondo regime).

Albeit this Kondo lattice peak sets in at around  $T_K$ , i.e.  $T_{\text{coh}} \approx T_K$  as mentioned above, it only slowly increases in height down to about 3 K  $\approx 0.1 T_{\text{coh}}$ , cf. tunneling conductance at 5.5 K in Fig. 3A. This, along with a further decrease of  $g(T)$  around zero bias, may explain why single-ion descriptions can often be applied to temperatures well below  $T_K$  despite neglected lattice Kondo effects [34, 35]. Only below about 3 K, the  $-6$  meV-peak gains considerably in height indicating dominant lattice Kondo correlations at these low temperatures. This is in line with magneto- [17] and thermal transport [36] investigations. In particular, the comparison of the STS data with thermopower measurements indicates the formation of a medium-heavy Fermi liquid down to about 3 K while strong non-Fermi liquid behavior sets in only below this temperature. Apparently, quantum criticality only sets in if there is sufficient buildup of lattice Kondo correlations at low enough temperatures [6]. A similar conclusion is suggested by resonant angle-

resolved photoemission spectroscopy on CeRhIn<sub>5</sub> [37].

STS was also conducted at 0.3 K for magnetic fields applied  $B \parallel c$ , see exemplary data for  $B = 9$  T in Fig. 3B. It should be noted that renormalized band structure calculations [33] predict a smooth quasiparticle disintegration up to well above 30 T in YbRh<sub>2</sub>Si<sub>2</sub> while AF order is already suppressed at  $B \approx 0.6$  T for  $B \parallel c$ . The position in energy of the Kondo lattice signature peak at  $-6$  meV is not influenced by applying a magnetic field, further supporting its attribution. After background subtraction it can be well fitted by a Gaussian, cf. inset of Fig. 3B. The width of the Gaussian fit is somewhat reduced at  $B = 1$  T compared to peak widths at zero field and at several Tesla. Here we note that a field magnitude of 1 T is close to the  $T^*$ -line (cf. Fig. 1) for  $T = 0.3$  K and  $B \parallel c$ . Therefore, the reduced peak width at  $B = 1$  T is consistent with a reduced quasiparticle weight related to quantum criticality, see also Fig. 4C. However, these STS data on their own do not allow to distinguish between different scenarios for quantum criticality and should be extended to lower temperatures.

Consequently, the question concerning the nature of the ‘local’ QCP in YbRh<sub>2</sub>Si<sub>2</sub> and the associated critical excitations remains. To answer this question, combined thermal and electrical transport investigations on YbRh<sub>2</sub>Si<sub>2</sub> single crystals were carried out down to 25 mK at zero field, close to  $B_N$  and up to  $B = 1$  T ( $\gg B_N$ ) [38]. Subsequently, Pourret et al. were able to extend such measurements down to even 8 mK [39]. The main quantity to study in this context is the Lorenz number  $L = \rho\kappa/T$ , where  $\rho$  is the electrical resistivity and  $\kappa$  the thermal conductivity. By defining the thermal resistivity as  $w = L_0T/\kappa$ , with  $L_0 = (\pi k_B)^2/3e^2$  being Sommerfeld’s constant, the Lorenz ratio  $L(T)/L_0$  can be written as  $L/L_0 = \rho/w$ . If the Wiedemann-Franz law is valid ( $L(T \rightarrow 0)/L_0 = 1$ ), which strictly holds for elastic scattering only, the *residual* electrical and thermal resistivities turn out to be identical:  $\rho_0/w_0 = 1$ .

Very different phenomena can cause a violation of this law: (i) Fermionic excitations like spinons, i.e., charge-neutral heat carriers, may lead to  $L(T \rightarrow 0)/L_0 > 1$ . This was indeed concluded from measurements on, e.g., LiCuVO<sub>4</sub> [40]. (ii) Alternatively, an enhanced  $w(T)$  can lead to  $L/L_0 < 1$ , as frequently observed at *finite* temperature with dominating inelastic scatterings of the charge carriers, like the ones from acoustic phonons. In the zero-temperature limit, however, inelastic scatterings have to disappear. To our knowledge, before 2012 this latter kind of violation of the Wiedemann-Franz law,  $L(T \rightarrow 0)/L_0 < 1$ , has never been convincingly established. For example, for the quasi-two-dimensional (2D) heavy-fermion metal CeCoIn<sub>5</sub>, where an AF QCP was suspected [41, 42] but not identified,  $L(T)/L_0$  was extrapolated to about 0.8 as  $T \rightarrow 0$  for  $c$ -axis transport at  $B \approx B_{c2} \approx 5$  T, while it approaches  $L(T)/L_0 \approx 1$  for in-plane ( $\perp c$ ) transport [43]. This result was ascribed to the action of anisotropic spin fluctuations, although

as  $T \rightarrow 0$ , spin fluctuations as bosonic excitations must disappear as well. Subsequently, the observations by Tanatar et al. could be consistently explained within the framework of quasi-2D transport [44].

In the following, we describe the violation of the Wiedemann-Franz law in YbRh<sub>2</sub>Si<sub>2</sub> with the aid of Fig. 4, see also [45]. As shown in Fig. 4A at  $B = 0$  and 0.07 T,  $L(T)/L_0 \approx 0.87$  in an extended temperature window ( $0.1 \text{ K} < T < 0.5 \text{ K}$ ) [39]. In this  $T$ -range, the underlying electrical and thermal resistivities depend linearly on  $T$ , so that the electronic Lorenz ratio  $L_{el}/L_0$  is temperature-independent. While for  $\rho(T)$  the ‘strange-metal’ behavior persists to the lowest accessible temperature, and most likely to absolute zero, an additional bosonic contribution  $\kappa_m(T)$  (by magnons at  $B = 0$ , resp. paramagnons at  $B = 0.07$  T) is added to the electronic thermal conductivity  $\kappa_{el}(T)$  at  $T \leq 0.1$  K which means that here, the total thermal resistivity  $w(T) = [\kappa_{el}(T) + \kappa_m(T)]^{-1}$  drops, and a distinct upturn develops in  $L(T)/L_0$ , as clearly seen in Fig. 4A. Because of its bosonic nature, this additional term has to vanish as  $T \rightarrow 0$ , whereby it must pass over a maximum below the low- $T$  limit of the experiments (8 mK). The (constant) low- $T$  value of  $L_{el}/L_0 \approx 0.87$ , displayed in Fig. 4A over an extended temperature window, is also derived from the minimum value of the  $L(B)/L_0$  isotherm for  $T = 0.1$  K, the lowest temperature at which no interfering paramagnon contribution to  $\kappa(T)$  exists (red data points in Fig. 4B). These data were obtained with a different set up on a different single crystal. We thus conclude that the ratio  $\rho_0/w_0 = \rho_0/w_{el,0}$  is reduced by about 10% compared with unity, the value expected from the Wiedemann-Franz law. Fig. 4B demonstrates that below 1 K, the Lorenz ratio is generally less than unity which implies predominating inelastic scattering processes, i.e., the ordinary small-angle electron-electron and electron-spin fluctuation scatterings. As already mentioned, in this low-temperature range, a broad minimum shows up in the  $L(B)/L_0$  isotherms displayed in the figure, which points to *an additional inelastic scattering process*. This minimum is found to occur around the  $T^*(B)$ -line and to become narrower upon cooling. We therefore consider it to represent the dynamical origin of local quantum criticality in YbRh<sub>2</sub>Si<sub>2</sub> by ascribing it to scatterings that are associated with the transformation between a small and a large Fermi surface, which coexist on either side of  $T^*(B)$  all the way down to the QCP ( $T = 0, B = B_N$ ). As displayed in Fig. 4C, the quasiparticle weights on both sides are smoothly vanishing as  $T \rightarrow 0$ , whereby the minimum in  $L(B)/L_0$  becomes a delta function, resulting from *fermionic* quantum critical fluctuations (which is a rare case, as in most scenarios quantum critical fluctuations are of *bosonic* origin). Apparently, these critical fluctuations are instrumental to enhance the residual thermal resistivity by about 10% over its electrical counterpart.

Several groups have reported very similar experimental data compared with those by [38], but questioned the

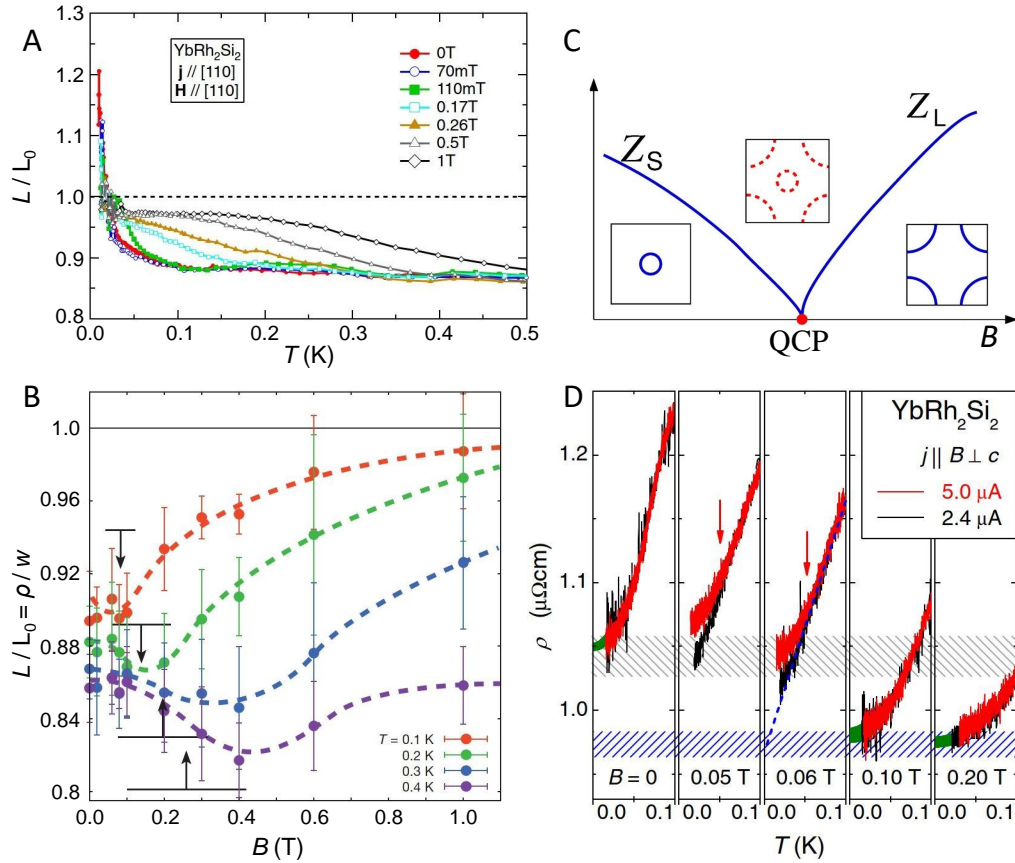


FIG. 4. **(A)** Lorenz ratio  $L(T)/L_0$  vs  $T$  for an YbRh<sub>2</sub>Si<sub>2</sub> single crystal at  $B = 0$  and at various finite fields  $B \perp c$ . Reproduced with permission from [39], Copyright (2014) The Physical Society of Japan. **(B)**  $L(T)/L_0$  vs  $B$  ( $\perp c$ ) isotherms,  $T \geq 0.1$  K (paramagnetic regime, purely electronic heat transport, no bosonic contribution to  $\kappa$ ). Reproduced from [38]. **(C)** Schematic sketch showing coexistence of small and large Fermi surfaces. Reproduced from [38]. **(D)**  $B_N = 0.059$  T. Black (small  $j$ ): no heating.  $B = 0$ ,  $[\rho(T) - \rho_{01}] = A_1 T^2$ ;  $B = 0.2$  T,  $[\rho(T) - \rho_{02}] = A_2 T^2$  (extrapolations to  $T = 0$  shown in green) with  $\rho_{01} > \rho_{02}$  (different carrier densities, small vs large FS).  $A_1 > A_2$  (see Fig. 2B).  $B = 0.05$  T ( $\leq B_N$ ) resp.  $B = 0.06$  T ( $\geq B_N$ ),  $[\rho(T) - \rho_{01}] \approx [\rho(T) - \rho_{02}] \approx A'T$ ; red (large  $j$ ): heating on the approach of the QCP due to additional inelastic scatterings discussed in the text. Reproduced from [46].

interpretation sketched above. The key problem is the correct treatment of the bosonic term  $\kappa_m(T)$ . This term was just ignored by [47, 48], i.e., here the measured thermal conductivity was erroneously regarded as the electronic contribution in the whole low-temperature range of the experiments, down to 40 mK. On the other hand, [49], who gave a detailed interpretation of the data previously published by [39], consider  $\kappa_m(T)$  to set in at a temperature as low as 30 mK, although the data [39] clearly prove this to occur already at about 0.1 K (see Fig. 4A). Therefore, on extrapolating the data to  $T = 0$  from just above 30 mK where  $\kappa_m(T)$  dominates, they miss the intrinsic value  $L_{el}(T \rightarrow 0)/L_0 \approx 0.9$  and instead obtain accidentally  $\approx 0.97$ . This leads to their false claim that the Wiedemann-Franz law holds in YbRh<sub>2</sub>Si<sub>2</sub>. A violation of the Wiedemann-Franz law was subsequently also reported for another heavy-fermion metal, YbAgGe [50].

In Fig. 4D, the conclusions drawn from the heat-

conduction study discussed above are nicely confirmed by results of measurements of the electrical resistivity [51]. Close to the critical field  $B_N = 59$  mT and at sufficiently low temperatures, the sample under investigation becomes heated by a moderate current due to its deteriorated heat conductivity. No heating is observed when applying a low enough current. Away from  $B_N$ , in the AF phase at  $B = 0$  as well as in the paramagnetic phase at 0.1 and 0.2 T, the resistivity follows the Fermi liquid-type  $T^2$ -dependence, independent of the size of the here investigated currents. Upon approaching  $B_N$  from either side, at the lowest accessible temperatures ‘strange-metal’ behavior, characteristic of the local QCP, is observed at low current. If these linear  $T$ -dependences of  $\rho(T)$  obtained at  $2.4 \mu\text{A}$  are extrapolated to  $T = 0$ ,  $\rho(T)$  ends up at very different values of the residual resistivity. In particular, the so extrapolated  $\rho_0$  values match nicely with those obtained by extrapolating the Fermi liquid-type  $T^2$ -dependences of  $\rho(T)$  found at  $B = 0$



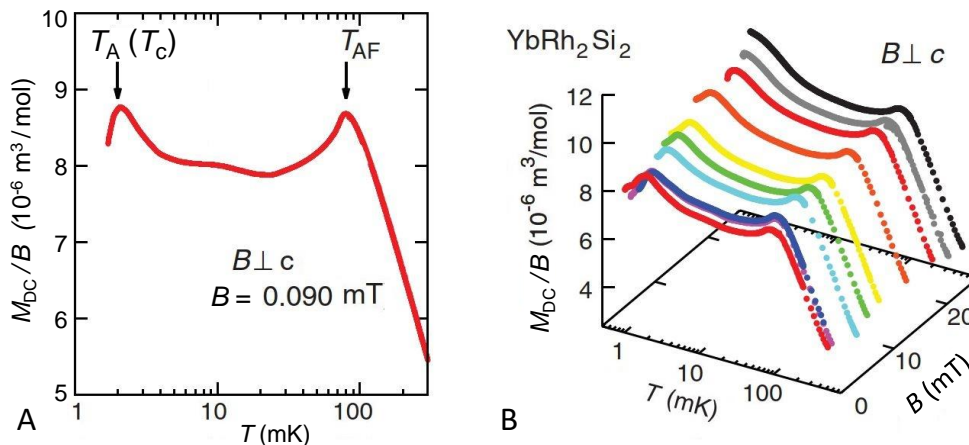


FIG. 5. Field-cooled (fc) DC magnetization  $M_{DC}$ , normalized at 1.1 mT, in dependence on temperature  $T$  for magnetic field  $B \perp c$ . After cooling the sample at the magnetic measuring field  $B$  to below 1 mK, the magnetization curve was taken on the warmup of the nuclear stage. (A)  $B = 0.090$  mT. (B)  $B \leq 23$  mT. Reproduced from [1].

and way above  $B_N$ , respectively. We consider this jump in  $\rho_0$  as a direct visualization of the abrupt change in the charge-carrier density of  $\text{YbRh}_2\text{Si}_2$  on field tuning through the Kondo-destroying QCP.

## II. COMPETITION BETWEEN NUCLEAR AND PRIMARY $4f$ -ELECTRONIC ORDER, EMERGENCE OF HYBRID A-PHASE AND SUPERCONDUCTIVITY

When  $\text{YbRh}_2\text{Si}_2$  single crystals were investigated by resistivity measurements at  $T > 10$  mK, and specific-heat as well as susceptibility measurements at  $T > 18$  mK, no superconductivity could be detected [25]. The most natural explanation for this is that superconductivity becomes suppressed by the AF order which forms at  $T_N = 70$  mK. To find out whether superconductivity in  $\text{YbRh}_2\text{Si}_2$  shows up at  $T \leq 10$  mK, magnetization, susceptibility and specific-heat measurements have been carried out down to temperatures as low as 0.8 mK by using a nuclear demagnetization cryostat providing a base temperature of 400  $\mu\text{K}$  [1]. Here, a total of 5 different single crystals was investigated. In Fig. 5A, the temperature dependence of the field-cooled (fc) DC-magnetization, measured at a magnetic field of 0.09 mT, reveals two phase-transition anomalies at  $T_N \approx 70$  mK and  $T_A$  ( $T_c$ )  $\approx 2$  mK. While the peak at 70 mK illustrates the AF  $4f$ -electronic transition, the one at 2 mK marks the transitions into both nuclear-dominated hybrid AF order (‘A phase’) and heavy-fermion superconductivity, as discussed below. A blow-up of the data near the 2 mK-peak at fields below 4 mT indicates that the onset of hybrid order precedes that of superconductivity, with  $T_A - T_c$  being less than  $0.1T_A$  [1]. Fig. 5B illustrates how these phase-transition anomalies evolve with increasing magnetic field. The position of the low-temperature

anomaly becomes gradually reduced until the latter cannot be resolved anymore above 23 mT, whereas  $T_N$  is robust in this whole field range. Clearly resolved is an increase in field-cooled magnetization,  $fc\text{-}M_{DC}(T)$ , upon cooling to below about 20 mK, which indicates a weakening of the staggered magnetization in the primary AF phase. At  $T \approx 10$  mK, a significant decrease in the absolute slope of  $fc\text{-}M_{DC}(T)$  is observed.

Figure 6A displays the zero-field-cooled (zfc-) and  $fc\text{-}M_{DC}(T)$  curves taken up to  $B = 0.418$  mT in a specially shielded setup (different from the one used to obtain the data of Fig. 5). The data registered at the lowest field,  $B = 0.012$  mT, illustrate how the experiment was performed: one starts at  $T > 10$  mK by cooling the sample in zero field to the lowest temperature,  $T = 0.8$  mK. Then, the field is applied and the zfc curve is recorded on warming to above 10 mK. Cooling again with field applied yields the fc curve. The  $zfc\text{-}M_{DC}(T)$  curve, which separates abruptly from the fc curve at  $T \approx 10$  mK, indicates a shielding signal which is increasing almost linearly upon cooling and assumes a value of not more than 20% just above  $T_c = 2$  mK. This is followed by a sharp, pronounced drop at  $T_c$  and a robust diamagnetic response at  $T \leq 1$  mK. These data are well reproduced by the results of the AC susceptibility obtained under nearly zero-field conditions, Fig. 6B. In the  $\chi_{AC}(T)$  data partial shielding below  $T \approx 10$  mK and the AF phase transition at  $T_N \approx 70$  mK are resolved as well.

We now turn to the peak in the  $fc\text{-}M_{DC}(T)$  curve at 2 mK which reveals a pronounced decline  $\Delta M$  of about  $0.075 \mu_B$  per Yb down to 0.8 mK (Fig 5A). As will be discussed below, about 25% of this decline on the low- $T$  side of the 2 mK-peak should be attributed to the onset of the nuclear- $4f$  electronic hybrid ‘A-phase’, leaving about 75% of this being due to the Meissner effect. This corresponds to a Meissner volume amounting to only about 2% of the full shielding

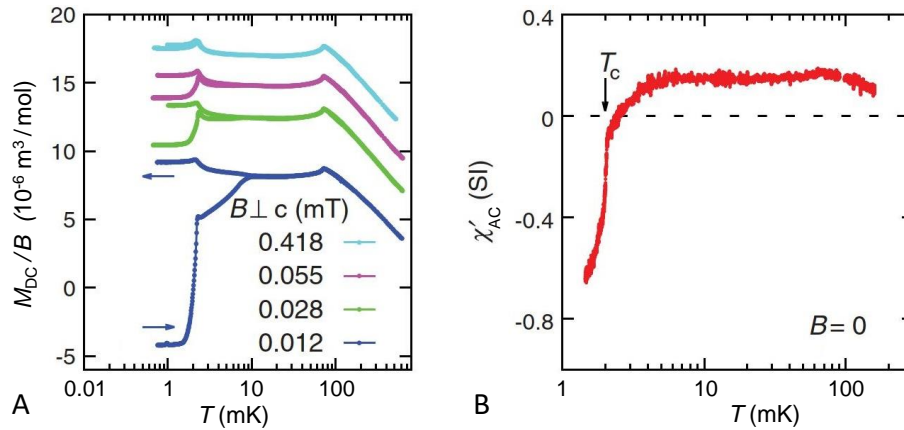


FIG. 6. **(A)** *fc*- and *zfc*- $M_{DC}(T)$  curves, normalized to 1.1 mT and offset for the sake of clarity, between 0.012 and 0.418 mT. The data were taken in a special measuring cell which allowed for the compensation of the earth field to obtain a smallest magnetic measuring field of 0.012 mT. Note that the vertical scale is larger by more than a factor of 5 compared to that in Fig. 5A. **(B)** Real part of the AC susceptibility  $\chi'_{AC}(T)$  at  $B \approx 0$ . Reproduced from [1].

signal which seems to be quite a small value; however, owing to vortex pinning this is typical for bulk type-II superconductors. After destroying the pinning centers by powdering and subsequent annealing, the sample should exhibit a substantially increased Meissner volume when measured below the lower critical field  $B_{c1}$ , see, e.g., [52, 53]. As also inferred from Fig. 6A, the shielding signal in *zfc*- $M_{DC}(T)$  has become extremely weak at a field as low as 0.418 mT, cf. the discussion below. By contrast, the jump in *fc*- $M_{DC}(T)$ ,  $\Delta M$ , is robust, hinting at the existence of *bulk* superconductivity with  $T_c \geq 0.8$  mK up to  $B \leq 23$  mT, see Fig. 5B.

The coefficient of the molar spin specific heat,  $\delta C(T)/T$ , obtained after subtracting a huge nuclear quadrupolar contribution (for  $B = 0$ ) from the raw data taken at 2.4 mT, is shown below 6 mK in Fig. 7A.  $\delta C(T)$  mainly consists of the contributions by the Yb-derived nuclear spins ( $S = 1/2$  for  $^{171}\text{Yb}$  ions with a natural abundance of 14.3% as well as  $S = 5/2$  for  $^{173}\text{Yb}$  ions with 16.1% abundance). Note that neither the  $^{100}\text{Rh}$  nor the  $^{29}\text{Si}$  nuclear spins contribute to the specific heat above  $T = 1$  mK, because they assume their full Zeeman entropies already below this temperature. In addition to the nuclear spin contributions, there is a small one by the  $4f$ -electronic spins,  $C_{4f}(T)$ . Since the effect of a magnetic field on the nuclear quadrupole contribution is only of higher order, one can use these  $\delta C(T)/T$  data, subtracted by  $C_{4f}(T)/T$ , to estimate the molar Yb-derived nuclear spin entropy  $S_{I,\text{Yb}}(T)$  (for  $B = 2.4$  mT). Clearly seen in Fig. 7A is a huge, broadened phase-transition anomaly of mean-field type. The latter can be replaced, under conservation of entropy, by a jump which yields a phase transition temperature of  $T_A = 2$  mK (at  $B = 2.4$  mT) and a jump height  $\Delta C/T_A$  of  $\approx 1700$  J/K<sup>2</sup>mol. This exceeds  $\Delta C/T_c$  observed at the transition temperature of typical heavy-fermion superconductors by more than a factor of 1000 and indicates that the A-

phase transition is predominantly due to nuclear degrees of freedom. Since an additional measurement at 59.6 mT revealed  $T_A$  to be shifted to below the lowest accessible temperature of 0.8 mK, this  $T_A$ -anomaly marks the transition into a state of antiferromagnetically ordered nuclear spins. In the inset of Fig. 7A,  $\delta C(T)/T$  is displayed on a largely expanded vertical scale between 6

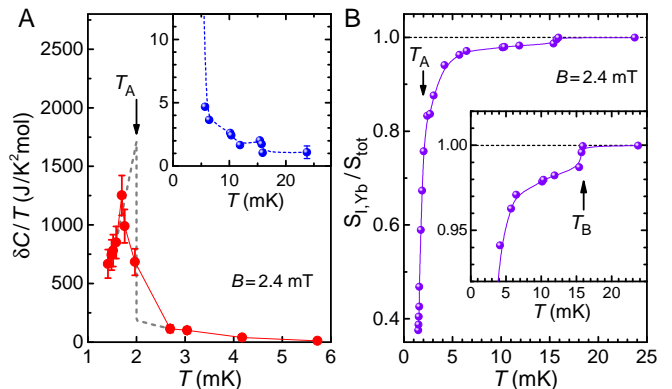


FIG. 7. **(A)** Molar spin specific heat of  $\text{YbRh}_2\text{Si}_2$  in an external magnetic field  $B = 2.4$  mT plotted as  $\delta C/T$  vs  $T$  at  $T < 6$  mK. The data were obtained by the common heat-pulse as well as the relaxation methods with the *fc*- $M_{DC}(T)$  dependence of  $\text{YbRh}_2\text{Si}_2$  used as an internal thermometer. In the latter case, the heat capacity  $\tilde{C}$  (including addenda contributions) could be determined by the relaxation time  $\tau = \tilde{C} R_{\text{th}}$ , with  $R_{\text{th}}$  being the thermal resistance of the ‘weak link’ (between sample and nuclear stage). For details, see [1]. The inset shows the same quantity on a smaller scale for  $T < 30$  mK. **(B)** Yb-derived nuclear spin entropy  $S_{I,\text{Yb}}/S_{\text{tot}}$  vs.  $T$  in units of  $S_{\text{tot}}$  where  $S_{\text{tot}}$  is its value at sufficiently high  $T$ . Inset: Zoom into the same data at  $T \geq 4$  mK to emphasize the jump at  $T_B$ .

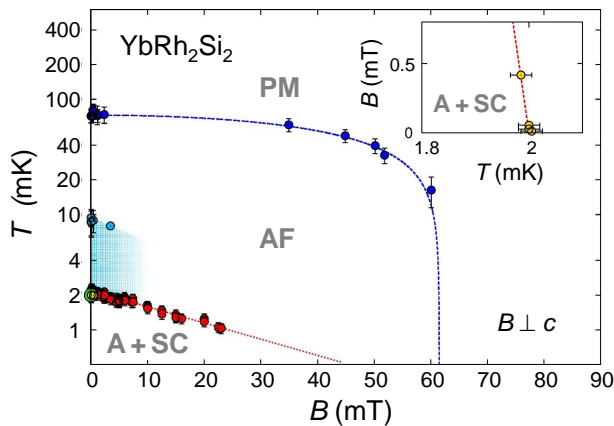


FIG. 8. Phase diagram of  $\text{YbRh}_2\text{Si}_2$ . Dark blue dots and line: boundary of the primary AF order. Light blue dots and shaded area: partial superconducting shielding in previously labelled ‘B-phase’, i.e., in insulated droplets of A-phase which form below  $T_B \approx 16$  mK, see text. Red data points: Position of low- $T$  peak in  $fc\text{-}M_{\text{DC}}(B)$ , see Fig. 5. Green circle: superconducting  $T_c$  at  $B = 0$  from  $\chi_{\text{AC}}(T)$ , see Fig. 6B. Yellow circles: superconducting  $T_c$  from  $zfc\text{-}M_{\text{DC}}(T)$ , Fig. 6A, blown up in the inset to illustrate the huge absolute value of the initial slope of  $B_{c2}(T)$  at  $T_c$ ,  $|B'_{c2}| \approx 25$  T/K. Figure adapted from [1].

– 23 mK, which now contains additional (in comparison to [1]) data for  $T > 12$  mK. At  $T \geq 18$  mK, where all nuclear spin components are negligible, these data agree well with previous results for  $C_{4f}(T)/T$  [25], cf. Fig. 2A. The anomaly visible at  $T_B \approx 16$  mK can also be recognized in Fig. 7B, where the temperature dependence of the entropy of the Yb-derived nuclear spins,  $S_{\text{I,Yb}}(T)$ , is displayed in units of its total (high- $T$ ) value,  $S_{\text{tot}}$ . This anomaly shall be discussed in more detail in the following section.

The temperature-magnetic field phase diagram in Fig. 8 indicates the various low- $T$ , low- $B$  phases of  $\text{YbRh}_2\text{Si}_2$ , i.e., the primary AF phase (blue dots and dashed line), the so-called ‘B-phase’ (light blue shading), the A-phase and superconductivity whose transition temperatures are closely spaced and jointly displayed by the red dots, designating the positions of the low-temperature peaks in  $fc\text{-}M_{\text{DC}}(T)$ , see Fig. 5. The green symbol at  $B = 0$  represents the superconducting phase transition observed in  $\chi_{\text{AC}}(T)$ , and the yellow ones, partly hidden by the former, denote the positions of the pronounced shielding signals registered at very low fields by  $zfc\text{-}M_{\text{DC}}(T)$  (Fig. 6A). These latter transition temperatures are plotted as a function of field in the inset, yielding the absolute initial slope of the upper critical field curve at  $T = T_c$ ,  $|dB_{c2}(T)/dT| = |B'_{c2}| \approx 25$  T/K. An identical value was obtained from the  $fc\text{-}M_{\text{DC}}(T)$  data at very low fields [1]. The large magnitude of  $|B'_{c2}|$  is typical for heavy-fermion superconductors, based upon the ordinary  $4f$ -electronic Kondo effect [54]. If the giant anomaly in  $\delta C(T)/T$

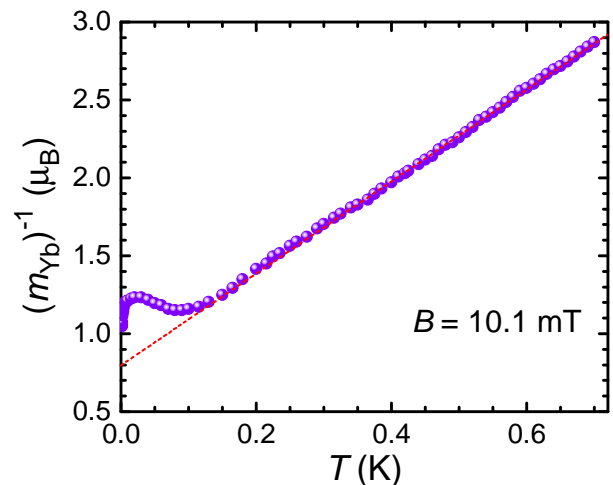


FIG. 9. Curie Weiss fit,  $\mu_B/m_{\text{Yb}}$  vs. temperature at  $B = 10.1$  mT. For  $T \rightarrow 0$  a saturation moment  $m_{\text{sat}} = 1.24 \mu_B$  is estimated. The Weiss temperature  $\theta \approx -0.27$  K agrees well with the result reported by [25] and illustrates dominant AF correlations at low temperature [57].

displayed in Fig. 7A manifested rather a superconducting than a nuclear-ordering transition, one would deal with super-heavy, almost localized, quasiparticles which were originating in a ‘nuclear Kondo effect’ [55]. In this case, the spins of the conduction electrons would rather screen the Yb-derived nuclear than the  $4f$ -electronic spins. This scenario cannot be at play as it would result in an almost infinite slope  $|B'_{c2}|$ .

One can derive the effective  $g$ -factor of the A-phase,  $g_{\text{eff}} \approx 0.051$ , from the ratio of the transition temperature  $T_A(B = 0) = 2.3$  mK and the critical field  $B_A(T \rightarrow 0) \simeq 45$  mT (Fig. 8). Using the in-plane  $4f$ - $g$ -factor of  $\text{YbRh}_2\text{Si}_2$ ,  $g_{4f} = 3.5$  [56], one finds the A-phase to represent hybrid AF order comprising a dominant ( $\approx 98.5\%$ ) nuclear component and a tiny  $4f$ -electronic component of  $\simeq 1.5\%$ , with a staggered moment of  $m_J \simeq 0.018 \mu_B$ . This is obtained with the aid of the ( $T \rightarrow 0$ ) saturation moment,  $1.24 \mu_B$ , as estimated from a Curie-Weiss fit to the  $fc$ -magnetization data taken in the paramagnetic regime at an external field of 10.1 mT, see Fig. 9. The staggered moment  $m_J$  exceeds significantly that of the primary AF phase,  $m_{\text{AF}} \approx 0.002 \mu_B$  [14] which may explain the ‘re-entrant AF order’ at very low temperatures as reported by [58] based on measurements of Nyquist noise. We note that a pure nuclear phase transition would not be resolved in our magnetization measurements because of the very small nuclear moment. Therefore, one can state that the 2 mK-peak in  $fc\text{-}M_{\text{DC}}(T)$  originates in the tiny  $4f$ -component of the hybrid A-phase (and additionally, to a larger part in the Meissner signal of the superconducting transition), while the huge anomaly in the specific-heat coefficient shown in Fig. 7A is only due to the Yb-derived nuclear spin states. We infer from the red data points shown in Fig.



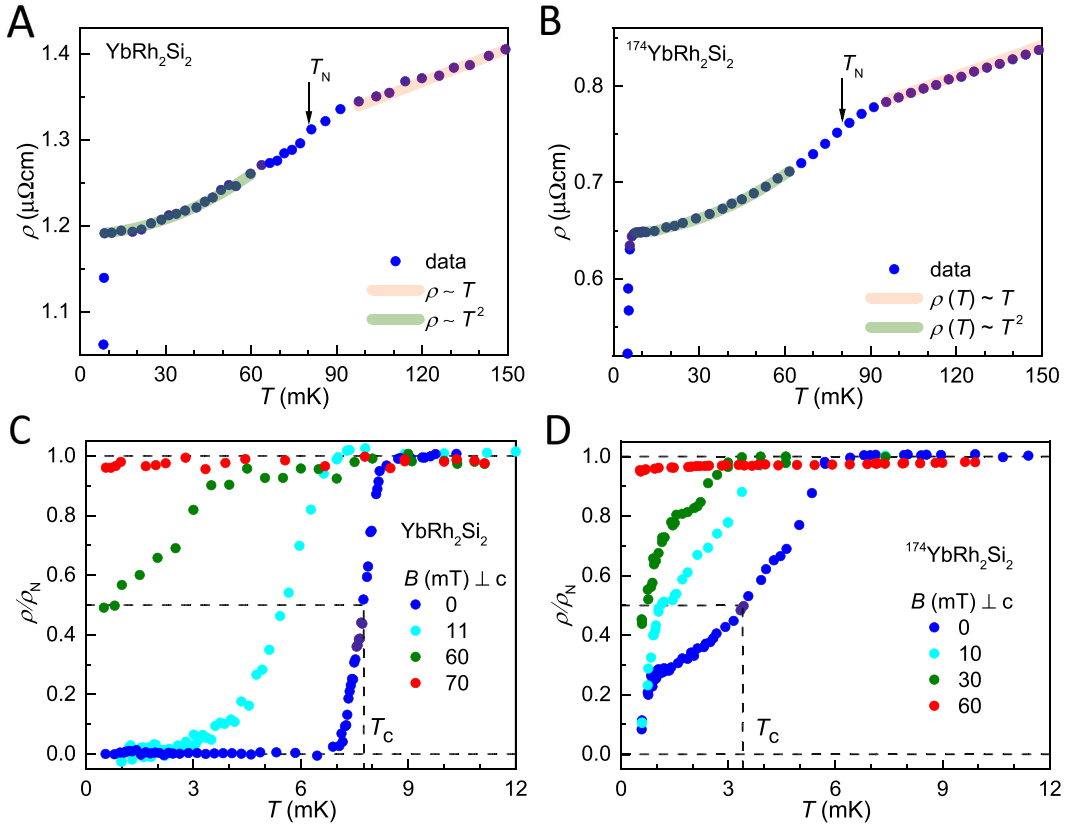


FIG. 10. Electrical resistivity as a function of temperature for (A), (C)  $\text{YbRh}_2\text{Si}_2$  and (B), (D)  $^{174}\text{YbRh}_2\text{Si}_2$  at  $B = 0$  and various applied fields. Reproduced from [2] under a Creative Commons Attribution 4.0 International License. Copyright 2021, The Authors, published by Springer Nature.

8 and the results of Fig. 5B that the existence range for bulk superconductivity is most likely extended to fields in excess of 23 mT where the values of  $T_c$  are below 0.8 mK.

Measurements of the electrical resistivity at ultra-low temperatures are extremely difficult in view of the unavoidable contact resistances which may easily heat up the sample. Recently, Nguyen et al. were successful in performing such measurements on  $\text{YbRh}_2\text{Si}_2$  single crystals down to 0.5 mK [2]. Figure 10 reproduces their results on a pristine sample of  $\text{YbRh}_2\text{Si}_2$  (A, C) as well as on a single crystal with nominally 100 at% of  $^{174}\text{Yb}$  ions which do not carry nuclear spins (denoted as  $^{174}\text{YbRh}_2\text{Si}_2$  in B, D). This latter sample had been prepared and intensively studied by [59]. For both single crystals the onset of the primary AF order at  $T_N = 70$  mK is resolved, see Figs. 10A and B, as is the superconducting transition with a (mid-point)  $T_c = 7.9$  mK, following an onset at  $\simeq 9$  mK, for the  $\text{YbRh}_2\text{Si}_2$  crystal and an onset at about 5 mK for the  $^{174}\text{YbRh}_2\text{Si}_2$  crystal (Figs. 10C and D). Within the resolution of the experiments, the resistivity reaches  $\rho = 0$  at about 6.5 mK for the former sample (Fig. 10C). In case of the nominally nuclear-spin free  $^{174}\text{YbRh}_2\text{Si}_2$  sample, the onset of superconductivity at 5 mK is followed by a broadened 75% decrease of  $\rho(T)$ , which starts to decline

in a substantially steeper fashion at about 1 mK, without reaching zero at the low- $T$  limit of 0.5 mK, suggesting  $\rho = 0$  at around 0.3 – 0.4 mK (Fig. 10D). Under external magnetic field the transitions are shifted to lower temperatures. As shown in Fig. 10C, for the  $\text{YbRh}_2\text{Si}_2$  sample, the transition is broadened at  $B = 11$  mT, and zero resistivity is achieved at  $T \approx 2$  mK. Even at  $B = 60$  mT a residual, very broad and incomplete transition is recognized. The initial  $T_c(B)$  dependence is found to be relatively steep, implying an absolute initial slope of  $|B'_{c2}| \simeq 4.4$  T/K. The field dependence of  $T_c$  becomes flatter above  $B \approx 11$  mT. The finite-field data for the  $^{174}\text{YbRh}_2\text{Si}_2$  sample displayed in Fig. 10D show a field-induced reduction of the temperature range of the broad initial decline in  $\rho(T)$ . In addition, the temperature of 0.3 – 0.4 mK at which  $\rho(T)$  is likely to vanish, appears to be almost independent of field up to  $B = 30$  mT.

To put these new results in perspective, we wish to note that resistive transitions (at  $T_{c,\rho}$ ) commonly probe percolative superconductivity, with  $\rho(T)$  reaching zero when the first percolating path through the sample is formed. On the other hand, both  $\chi_{AC}(T)$  (with  $T_{c,\chi}$ ) and  $\text{zfc-}M_{DC}(T)$  provide shielding signals due to ‘networks of screening currents’ in the sample surface.

The thermodynamic (bulk-)  $T_c$  is obtained through transitions in the specific heat and/or the Meissner effect as measured by  $fc\text{-}M_{\text{DC}}(T)$  (with  $T_{c,M}$ ). For inhomogeneous superconductors one frequently finds  $T_{c,\rho} > T_{c,\chi} > T_{c,M}$ . In case of the Ce-based 115-superconductors with anisotropic transport owing to the delicate interplay of competition and coexistence between superconductivity and AF order, an exotic type of percolative (‘textured’) superconductivity has been reported [60]. For CeIrIn<sub>5</sub>, the thermodynamic  $T_c$  probed via specific heat is 0.4 K, while  $T_{c,\rho} = 1.2$  K [61].

In the YbRh<sub>2</sub>Si<sub>2</sub> sample, the onset of superconductivity at very low fields is observed at almost the same  $T_{c,\rho} \approx 8$  mK in measurements of both the electrical resistivity [2] and Nyquist noise [58]. In this exceptional case  $T_{c,\rho}$ , and even the onset temperature of the resistive transition, is *smaller* than  $T_{c,\chi} \approx 10$  mK. The resistivity study yields an absolute initial slope of  $B_{c2}(T)$  at  $T_c$ ,  $|B'_{c2}| \approx 4.4$  T/K discussed above, which is much smaller than the value 25 T/K based on  $zfc\text{-}$  and  $fc\text{-}M_{\text{DC}}(T)$  results, cf. the preceding Section II. In addition, the thermodynamic superconducting transition displayed by the low-temperature peak in  $fc\text{-}M_{\text{DC}}(T)$  is corroborated by abrupt and large shielding signals in both  $zfc\text{-}M_{\text{DC}}(T)$  and  $\chi_{\text{AC}}(T)$ , cf. Figs. 6A and B, respectively.

Concerning the <sup>174</sup>YbRh<sub>2</sub>Si<sub>2</sub> sample, we believe that (i) it contains a low, but finite, concentration of residual Yb ions with nuclear spins which give rise to a weakened hybrid A-phase order and, thus, weakened superconductivity, and (ii) YbRh<sub>2</sub>Si<sub>2</sub> free of nuclear spins would not be a superconductor, at least near  $B = 0$ . To check this, future studies of superconductivity of YbRh<sub>2</sub>Si<sub>2</sub> samples with enriched <sup>174</sup>Yb isotope should be assisted by high-precision mass spectrometry, which is required to determine the amount of residual nuclear spins.

A three-component Landau theory was applied in [1] to explain the development of two subsequent AF phase transitions at  $T_N$  and  $T_A$ . (Assuming two components, one would obtain only one phase transition). This theoretical treatment was based on the empirical knowledge that the  $4f$ -electronic spin susceptibility  $\chi_{4f}(\mathbf{Q})$  is highly anisotropic, exhibiting maxima at two wave vectors,  $\mathbf{Q}_{\text{AF}}$  and  $\mathbf{Q} = 0$ , and giving rise to the primary AF order and ferromagnetic correlations [62], respectively.

It is, therefore, natural to assume that a peak in  $\chi_{4f}(\mathbf{Q})$  exists at yet another finite wave vector  $\mathbf{Q}_1$ , different from  $\mathbf{Q}_{\text{AF}}$ . Along  $\mathbf{Q}_1$ , the RKKY interaction generates an order parameter  $\Phi_J$  among the  $4f$ -electronic spins and simultaneously an order parameter  $\Phi_I$  among the Yb-derived nuclear spins. According to the size of the effective  $g$ -factor discussed above,  $\Phi_I$  must be much larger than  $\Phi_J$ . As  $\Phi_J$  and  $\Phi_I$  exist at the same wave vector  $\mathbf{Q}_1$ , they are coupled bilinearly via  $-\lambda\Phi_J\Phi_I$ , where the coupling parameter  $\lambda \approx 25$  mK is related to the hyperfine coupling constant  $A_{\text{hf}}$  by  $\lambda \sim A_{\text{hf}} \approx 100$  T/ $\mu_B$ . As a result, one finds the transition temperature of the nuclear-dominated hybrid

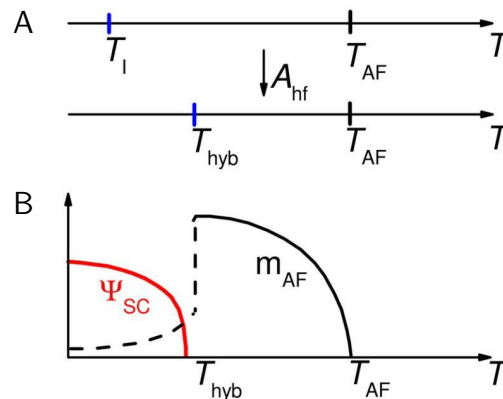


FIG. 11. Three component Landau theory: Phase transitions at  $T_{\text{AF}}$  and  $T_{\text{hyb}}$ . **(A)** Sketch of the two phase transitions associated with electronic and nuclear spin orders. (Top line) Without any hyperfine coupling ( $A_{\text{hf}}$ ), the electronic and nuclear spins are ordered at  $T_{\text{AF}}$  and  $T_I$ , respectively. (Bottom line) With hyperfine coupling,  $T_{\text{AF}}$  is not affected, but a hybrid nuclear and electronic spin order is induced at  $T_{\text{hyb}} \gg T_I$ . **(B)** Temperature evolution of the primary electronic spin order parameter ( $m_{\text{AF}}$ ) and the superconducting order parameter  $\Psi_{\text{SC}}$ .  $\Psi_{\text{SC}}$  is developed when  $m_{\text{AF}}$  is suppressed by the formation of hybrid nuclear and electronic spin order directly below  $T_{\text{hyb}}$ . Reproduced from [1].

A-phase  $T_{\text{hyb}} \approx \lambda^2 \chi_{4f}(\mathbf{Q}_1) / g_{4f}^2 \approx 1$  mK. Here, the value of the bulk susceptibility was taken for that of the unknown  $\chi_{4f}(\mathbf{Q}_1)$ . In view of this uncertainty, the agreement between the theoretical result for  $T_{\text{hyb}}$  and the experimental value  $T_A = 2$  mK is surprisingly good. Within the afore-described Landau treatment it may be assumed that the nuclear order parameter  $\Phi_I$  competes with the primary  $4f$ -electronic order parameter  $\Phi_{\text{AF}}$  that was found to be detrimental to superconductivity. Consequently, superconductivity sets in once the primary order  $\Phi_{\text{AF}}$  is suppressed, cf. Figure 11.

As this Landau theory is a mean-field theory, it does not treat short-range order. However, unique nuclear short-range order, as visualized by a significant temperature dependence of the nuclear spin entropy (Fig. 7B), apparently exists up to at least 16 mK and generates the nucleation of superconductivity at  $T \approx 10$  mK (Fig. 6A). In reality, as was inferred from Fig. 5A, the staggered magnetization of the primary AF phase,  $m_{\text{AF}}$ , starts to decrease already at 20 mK, rather than at  $T = T_{\text{hyb}}$ . As suggested in Fig. 11,  $m_{\text{AF}}(T)$  continues to decrease below  $T_{\text{hyb}}$  and may well vanish as  $T \rightarrow 0$ . This means, the QCP is located at (or very close to) zero external magnetic field. Interestingly, the transition from the primary AF order to superconductivity is of first order [1], similar to what was found for single-crystalline  $A/S$ -type CeCu<sub>2</sub>Si<sub>2</sub> [63].

In the following we summarize, and offer a—possibly oversimplified—explanation of, the multitude of puzzling

results achieved by the previous magnetic and calorimetric as well as the recent resistive measurements:

- i. Superconductivity in  $\text{YbRh}_2\text{Si}_2$  apparently exists in a wide field range almost up to  $B_A = 45$  mT, with the maximum  $T_c$  occurring at  $B = 0$  [1].
- ii. The  $T$ -dependence of  $\text{fc-}M_{\text{DC}}(T)$  displayed in Fig. 5A demonstrates that the staggered moment,  $m_{\text{AF}}$ , of the primary order starts to decrease already at about 20 mK, which is close to the temperature associated with the strength of the local Yb hyperfine interaction (25 mK). In addition, a significant  $T$ -dependence of the Yb-derived nuclear spin entropy,  $S_{\text{I,Yb}}(T)$ , is observed up to  $T_B \approx 16$  mK, where a distinct anomaly is visible in Fig. 7. The latter is associated with a rather sharp removal of a tiny fraction of about 1.5% of  $S_{\text{tot}}$ , the full value of  $S_{\text{I,Yb}}(T)$  at high temperatures. This can be ascribed to a corresponding small fraction of the Yb-derived nuclear spins which interact with the mean hyperfine field induced by the  $4f$ -electron spins [1] to create random and insulated A-phase regions which must be growing upon lowering the temperature.
- iii. The simultaneous onset of both a weak, but distinct shielding signal (Fig. 6) and a pronounced decline in the absolute slope of  $\text{fc } M_{\text{DC}}(T)$  (Fig. 5A) at  $T \approx 10$  mK are interpreted as manifesting the nucleation of superconductivity.
- iv. The network of superconducting islands turns out to be extremely fragile as the shielding signal is suppressed already by a very small external magnetic field (Fig. 6A).
- v. Upon further cooling, the resistivity reaches zero at about 6.5 mK. This can be reconciled with the above results in terms of the onset of superconducting percolation as mentioned before. The percolation initiates a considerably increasing strength of A-phase short-range order as illustrated by a pronounced increase of  $\text{fc-}M_{\text{DC}}(T)$  below 5 mK (Fig. 5A) and corroborated by a significant removal of the Yb-derived nuclear spin entropy from its maximum value  $S_{\text{tot}}$  (at  $T > T_B$ ) by 26% on cooling the sample down to  $T_A$  (Fig. 7B). Remarkably, the shielding signal due to the network of superconducting islands in the sample surface does not exceed 20% when cooling from  $T \approx 10$  mK to  $T \geq T_A$ , the temperature range previously called ‘B-phase’, cf. Fig. 8.
- vi. At  $T_A$  ( $= 2.3$  mK as  $B \rightarrow 0$ , see [1]), a second-order phase transition into long-range A-phase order takes place (Fig. 7A). The ordering of the Yb nuclear spins reaches a level of more than 60% already at 1.5 mK, see Fig. 7B. Nuclear-dominated hybrid order at elevated magnetic fields has yet

to be confirmed by future measurements of the specific heat. This should clarify whether the A-phase exists up to  $B_A \simeq 45$  mT, as indicated by the dotted red line in the phase diagram of Fig. 8, or even up to the quantum critical field  $B_N = 60$  mT, as suggested by the new resistivity results of [2] (Fig. 10). In the latter case, we conjecture the existence of not just two QCPs at  $B = B_N$  (vanishing of the primary AF order due to the applied magnetic field) and at  $B = 0$  (due to the competing A-phase). Rather, a phase boundary  $T_A(B)$  spanning the whole field range  $B < B_N$  would exist and most likely establish a *quantum critical line* between these two QCPs.

- vii. From the magnetization measurements [1], bulk superconductivity emerges at  $T_c = 2$  mK (Figs. 5A and 6A), slightly below  $T_A$ . Future  $\text{fc-}M_{\text{DC}}(T)$  measurements on annealed powder samples below the lower critical field  $B_{c1}$  are needed to confirm that bulk superconductivity indeed exists well below  $T_{c,\rho}$  at magnetic fields up to  $B \simeq B_A$ .

We should welcome future work by other groups to cross-check the above reasoning.

The new resistivity study by [2] suggests the existence of two separate superconducting regimes, at low and elevated fields, respectively. In view of the preceding discussion, we cannot concur with the proposal by Nguyen et al. that, at least in the low-field regime, Cooper pairing in  $\text{YbRh}_2\text{Si}_2$  is mediated by the critical fluctuations of the *field-induced* QCP at  $B_N$ : For, here the primary AF order is apparently suppressed by the competing nuclear order, allowing a quantum critical line to be established. Therefore, it is natural to consider the associated quantum critical fluctuations at *very low fields* being the driving force for the formation of Cooper pairs.

The origin of the superconductivity at elevated fields remains to be resolved. If here, the existence of the nuclear-dominated hybrid A-phase can be proven by future specific-heat experiments, the Cooper-pairing mechanism emphasized above in the low-field regime will most likely be operating as well. An alternative scenario proposed by [2] neglects the competition between the nuclear and primary  $4f$ -electronic orders and instead implies, as mentioned before, that the quantum critical fluctuations associated with the *field-induced* QCP at  $B_N = 60$  mT bring about the formation of superconductivity. As these critical fluctuations would be strongly impeded by the pair-breaking applied magnetic field, the competition between the field-induced quantum criticality and the destructive action of the magnetic field on the Cooper pairs causes a maximum  $T_c$  to occur well below  $B_N$ . [2] propose that superconductivity at elevated fields may be of the spin-triplet variety. While this would not have been a surprise had the quantum criticality been of nearly ferromagnetic (and conventional) type [64], how could spin-triplet pairing develop for Kondo-destroying type AF quantum criticality as is the case

in  $\text{YbRh}_2\text{Si}_2$ ? Insights into this question have come from theoretical studies near a Kondo-destroying QCP in antiferromagnetically coupled Kondo models [65]: They showed that significant Ising anisotropy, as it effectively arises under an external magnetic field in the easy-plane antiferromagnetically correlated  $\text{YbRh}_2\text{Si}_2$ , makes the spin-triplet pairing competitive.

### III. PERSPECTIVE

The discovery of superconductivity in  $\text{YbRh}_2\text{Si}_2$  at ultra-low temperatures opens up new dimensions. It expands the horizon of ultra-low temperature physics towards strongly correlated electronic matter in solids and conversely, it determines a new area of heavy-fermion physics by reaching down to ultra-low temperatures.

Up to now, heavy-fermion superconductivity has been detected in more than fifty  $f$ -electron compounds. Despite the fact that, compared with  $\text{PuCoGa}_5$ , exhibiting the record-high  $T_c$  of 18.5 K [66],  $\text{YbRh}_2\text{Si}_2$  shows a transition temperature which is lower by almost four decades, this may be called ‘high  $T_c$ ’—in the sense that  $T_c$  is limited by an enormously high ordering temperature of nuclear spins. This nuclear order paves the way for the superconductivity, not by actively helping in the Cooper-pair formation, rather by destroying the  $4f$ -electronic order below  $T_N = 70$  mK, which appears to be extremely hostile to superconductivity. The apparent competition between the nuclear and the  $4f$ -electronic orders results in an AF QCP at, or very close to,  $B = 0$ . Most likely, the latter—like its field-induced counterpart at  $B = B_N$ —is of the ‘local’ type, as inferred from the  $B = 0$  results of electrical and thermal transport as well as specific-heat measurements in the paramagnetic state as presented in Section I.

The ultra-low temperature work on  $\text{YbRh}_2\text{Si}_2$  strongly

supports the notion that superconductivity robustly develops in the vicinity of such a ‘partial-Mott’ QCP, as has been theoretically derived in Kondo-lattice models for a Kondo-destroying QCP [67] and experimentally evidenced from de Haas-van Alphen studies in high magnetic fields [23] and transport measurements [24] on pressurized  $\text{CeRhIn}_5$ . Therefore, the results on these two compounds provide the long-sought [68] link between unconventional superconductivity in heavy-fermion metals [69] and that occurring near a true Mott metal-insulator transition, e.g., in the cuprates [70] and organic charge-transfer salts [71].

### AUTHOR CONTRIBUTIONS

All authors contributed substantially to the discussion and revision of the manuscript.

### FUNDING

S.W. acknowledges support by the Deutsche Forschungsgemeinschaft through WI 1324/5-1.

### CONFLICT OF INTEREST STATEMENT

The authors declare that the research was conducted in the absence of any commercial or financial relationships that could be construed as a potential conflict of interest.

### ACKNOWLEDGMENTS

We are grateful for conversations with Manuel Brando, Ang Cai, Lei Chen, Piers Coleman, Haoyu Hu, Stefan Lausberg, Silke Paschen, John Saunders, Rong Yu and in particular with Qimiao Si for his insightful comments.

- 
- [1] E. Schubert, M. Tippmann, L. Steinke, S. Lausberg, A. Steppke, M. Brando, C. Krellner, C. Geibel, R. Yu, Q. Si, et al., *Science* **351**, 485 (2016).
  - [2] D. H. Nguyen, A. Sidorenko, M. Taupin, G. Knebel, G. Lapertot, E. Schubert, and S. Paschen, *Nat. Commun.* **12**, 4341 (2021).
  - [3] S. Wirth and F. Steglich, *Nat. Rev. Mat.* **1**, 16051 (2016).
  - [4] Q. Y. Chen, D. F. Xu, X. H. Niu, J. Jiang, R. Peng, H. C. Xu, C. H. P. Wen, Z. F. Ding, K. Huang, L. Shu, et al., *Phys. Rev. B* **96**, 045107 (2017).
  - [5] S. Ernst, S. Kirchner, C. Krellner, C. Geibel, G. Zwicknagl, F. Steglich, and S. Wirth, *Nature* **474**, 362 (2011).
  - [6] S. Seiro, L. Jiao, S. Kirchner, S. Hartmann, S. Friedemann, C. Krellner, C. Geibel, Q. Si, F. Steglich, and S. Wirth, *Nat. Commun.* **9**, 3324 (2018).
  - [7] G. R. Stewart, *Rev. Mod. Phys.* **73**, 797 (2001), *ibid.* **78**, 743-753 (2006).
  - [8] H. von Löhneysen, A. Rosch, M. Vojta, and P. Wölfle, *Rev. Mod. Phys.* **79**, 1015 (2007).
  - [9] P. Gegenwart, F. Steglich, and Q. Si, *Nature Phys.* **4**, 186 (2008).
  - [10] S. Sachdev, *Quantum phase transitions* (Cambridge University Press, 2011).
  - [11] U. Köhler, N. Oeschler, F. Steglich, S. Maquilon, and Z. Fisk, *Phys. Rev. B* **77**, 104412 (2008).
  - [12] O. Trovarelli, C. Geibel, S. Mederle, C. Langhammer, F. M. Grosche, P. Gegenwart, M. Lang, G. Sparn, and F. Steglich, *Phys. Rev. Lett.* **85**, 626 (2000).
  - [13] P. Gegenwart, J. Custers, C. Geibel, K. Neumaier, T. Tayama, K. Tenya, O. Trovarelli, and F. Steglich, *Phys. Rev. Lett.* **89**, 056402 (2002).
  - [14] K. Ishida, D. E. MacLaughlin, B.-L. Young, K. Okamoto, Y. Kawasaki, Y. Kitaoka, G. J. Nieuwenhuys, R. H. Heffner, O. O. Bernal, W. Higemoto, et al., *Phys. Rev.*

- B **68**, 184401 (2003).
- [15] P. Gegenwart, T. Westerkamp, C. Krellner, Y. Tokiwa, S. Paschen, C. Geibel, F. Steglich, E. Abrahams, and Q. Si, *Science* **315**, 969 (2007).
- [16] S. Paschen, T. Lühmann, S. Wirth, P. Gegenwart, O. Trovarelli, C. Geibel, F. Steglich, P. Coleman, and Q. Si, *Nature* **432**, 881 (2004).
- [17] S. Friedemann, N. Oeschler, S. Wirth, C. Krellner, C. Geibel, F. Steglich, S. Paschen, S. Kirchner, and Q. Si, *Proc. Natl. Acad. Sci. USA* **107**, 14547 (2010).
- [18] Q. Si, S. Rabello, K. Ingersent, and J. L. Smith, *Nature* **413**, 804 (2001).
- [19] P. Coleman, C. Pépin, Q. Si, and R. Ramazashvili, *J. Phys.: Condens. Matter* **13**, R723 (2001).
- [20] M. C. Aronson, R. Osborn, R. A. Robinson, J. W. Lynn, R. Chau, C. L. Seaman, and M. B. Maple, *Phys. Rev. Lett.* **75**, 725 (1995).
- [21] A. Schröder, G. Aeppli, R. Coldea, M. Adams, O. Stockert, H. von Löhneysen, E. Bucher, R. Ramazashvili, and P. Coleman, *Nature* **407**, 351 (2000).
- [22] H. von Löhneysen, T. Pietrus, G. Portisch, H. G. Schlager, A. Schröder, M. Sieck, and T. Trappmann, *Phys. Rev. Lett.* **72**, 3262 (1994).
- [23] H. Shishido, R. Settai, H. Harima, and Y. Ōnuki, *J. Phys. Soc. Jpn.* **74**, 1103 (2005).
- [24] T. Park, F. Ronning, H. Q. Yuan, M. B. Salamon, R. Movshovich, J. L. Sarrao, and J. D. Thompson, *Nature* **440**, 65 (2006).
- [25] J. Custers, P. Gegenwart, H. Wilhelm, K. Neumaier, Y. Tokiwa, O. Trovarelli, C. Geibel, F. Steglich, C. Pépin, and P. Coleman, *Nature* **424**, 524 (2003).
- [26] T. Westerkamp, Ph.D. thesis, Technical University Dresden, Germany (2009).
- [27] P. Wölfe and E. Abrahams, *Phys. Rev. B* **84**, 041101(R) (2011).
- [28] M. Taupin and S. Paschen (2022), *arXiv:2201.02820*.
- [29] S. Kirchner, S. Paschen, Q. Chen, S. Wirth, D. Feng, J. D. Thompson, and Q. Si, *Rev. Mod. Phys.* **92**, 011002 (2020).
- [30] S. Wirth, S. Ernst, R. Cardoso-Gil, H. Borrmann, S. Seiro, C. Krellner, C. Geibel, S. Kirchner, U. Burkhardt, Y. Grin, et al., *J. Phys.: Condens. Matter* **24**, 294203 (2012).
- [31] V. Alexandrov, P. Coleman, and O. Erten, *Phys. Rev. Lett.* **114**, 177202 (2015).
- [32] O. Stockert, M. M. Koza, J. Ferstl, A. P. Murani, C. Geibel, and F. Steglich, *Physica B* **378**, 157 (2006).
- [33] G. Zwicknagl, *J. Phys. Condens. Matter* **23**, 094215 (2011).
- [34] P. Coleman, P. W. Anderson, and T. V. Ramakrishnan, *Phys. Rev. Lett.* **55**, 414 (1985).
- [35] P. Sun and F. Steglich, *Phys. Rev. Lett.* **110**, 216408 (2013).
- [36] S. Hartmann, N. Oeschler, C. Krellner, C. Geibel, S. Paschen, and F. Steglich, *Phys. Rev. Lett.* **104**, 096401 (2010).
- [37] Q. Y. Chen, D. F. Xu, X. H. Niu, R. Peng, H. C. Xu, C. H. P. Wen, X. Liu, L. Shu, S. Y. Tan, X. C. Lai, et al., *Phys. Rev. Lett.* **120**, 066403 (2018).
- [38] H. Pfau, S. Hartmann, U. Stockert, P. Sun, S. Lausberg, M. Brando, S. Friedemann, C. Krellner, C. Geibel, S. Wirth, et al., *Nature* **484**, 493 (2012).
- [39] A. Pourret, D. Aoki, M. Boukahil, J.-P. Brison, W. Knafo, G. Knebel, S. Raymond, M. Taupin, Y. Ōnuki, and J. Flouquet, *J. Phys. Soc. Jpn.* **83**, 061002 (2014).
- [40] L. S. Parfen'eva, I. A. Smirnov, H. Misiorek, J. Mucha, A. Jezowski, A. V. Prokof'ev, and W. Assmus, *Phys. Solid State* **46**, 357 (2004).
- [41] S. Singh, C. Capan, M. Nicklas, M. Rams, A. Gladun, H.-O. Lee, J. F. DiTusa, Z. Fisk, F. Steglich, and S. Wirth, *Phys. Rev. Lett.* **98**, 057001 (2007).
- [42] S. Zaum, K. Grube, R. Schäfer, E. D. Bauer, J. D. Thompson, and H. von Löhneysen, *Phys. Rev. Lett.* **106**, 087003 (2011).
- [43] M. A. Tanatar, J. Paglione, C. Petrovic, and L. Taillefer, *Science* **316**, 1320 (2007).
- [44] M. F. Smith and R. H. McKenzie, *Phys. Rev. Lett.* **101**, 266403 (2008).
- [45] M. Smidman, O. Stockert, J. Arndt, G. M. Pang, L. Jiao, H. Q. Yuan, H. A. Vieyra, S. Kitagawa, K. Ishida, K. Fujiwara, et al., *Phil. Mag.* **98**, 2930 (2018).
- [46] F. Steglich, H. Pfau, S. Lausberg, S. Hamann, P. Sun, U. Stockert, M. Brando, S. Friedemann, C. Krellner, C. Geibel, et al., *J. Phys. Soc. Jpn.* **83**, 061001 (2014).
- [47] Y. Machida, K. Tomokuni, K. Izawa, G. Lapertot, G. Knebel, J.-P. Brison, and J. Flouquet, *Phys. Rev. Lett.* **110**, 236402 (2013).
- [48] J.-P. Reid, M. A. Tanatar, R. Daou, R. Hu, C. Petrovic, and L. Taillefer, *Phys. Rev. B* **89**, 045130 (2014).
- [49] M. Taupin, G. Knebel, T. D. Matsuda, G. Lapertot, Y. Machida, K. Izawa, J.-P. Brison, and J. Flouquet, *Phys. Rev. Lett.* **115**, 046402 (2015).
- [50] J. K. Dong, Y. Tokiwa, S. L. Bud'ko, P. C. Canfield, and P. Gegenwart, *Phys. Rev. Lett.* **110**, 176402 (2013).
- [51] S. Lausberg, Ph.D. thesis, Technical University Dresden, Germany (2013).
- [52] F. Steglich, J. Aarts, C. Bredl, W. Lieke, D. Meschede, W. Franz, and H. Schäfer, *Phys. Rev. Lett.* **43**, 1892 (1979).
- [53] U. Rauchschwalbe, W. Lieke, C. D. Bredl, F. Steglich, J. Aarts, K. M. Martini, and A. C. Mota, *Phys. Rev. Lett.* **49**, 1448 (1982).
- [54] W. Assmus, M. Herrmann, U. Rauchschwalbe, S. Riegel, W. Lieke, H. Spille, S. Horn, G. Weber, F. Steglich, and G. Cordier, *Phys. Rev. Lett.* **52**, 469 (1984).
- [55] P. Coleman (2015), private communication.
- [56] J. Sichelschmidt, V. A. Ivanshin, J. Ferstl, C. Geibel, and F. Steglich, *Phys. Rev. Lett.* **91**, 156401 (2003).
- [57] S. Hamann, J. Zhang, D. Jang, A. Hannaske, L. Steinke, S. Lausberg, L. Pedrero, C. Klingner, M. Baenitz, F. Steglich, et al., *Phys. Rev. Lett.* **122**, 077202 (2019).
- [58] J. Saunders (2018), invited Talk at 12th Intern. Conf. on Materials and Mechanisms of Superconductivity (M<sup>2</sup>S 2018), Beijing, China.
- [59] G. Knebel, R. Boursier, E. Hassinger, G. Lapertot, P. G. Niklowitz, A. Pourret, B. Salce, J. P. Sanchez, I. Sheikin, P. Bonville, et al., *J. Phys. Soc. Jpn.* **75**, 114709 (2006).
- [60] T. Park, H. Lee, I. Martin, X. Lu, V. A. Sidorov, K. Gofryk, F. Ronning, E. D. Bauer, and J. D. Thompson, *Phys. Rev. Lett.* **108**, 077003 (2012).
- [61] C. Petrovic, R. Movshovich, M. Jaime, P. G. Pagliuso, M. F. Hundley, J. L. Sarrao, Z. Fisk, and J. D. Thompson, *Europhys. Lett.* **53**, 354 (2001).
- [62] P. Gegenwart, J. Custers, Y. Tokiwa, C. Geibel, and F. Steglich, *Phys. Rev. Lett.* **94**, 076402 (2005).
- [63] O. Stockert, D. Andreica, A. Amato, H. S. Jeevan, C. Geibel, and F. Steglich, *Physica B* **374-375**, 167 (2006).



- [64] Y. Li, Q. Wang, Y. Xu, W. Xie, and Y. f. Yang, Phys. Rev. B **100**, 085132 (2019).
- [65] H. Hu, A. Cai, L. Chen, and Q. Si (2021), *arXiv:2109.12794*.
- [66] J. L. Sarrao, L. A. Morales, J. D. Thompson, B. L. Scott, G. R. Stewart, F. Wastin, J. Rebizant, P. Boulet, E. Colineau, and G. H. Lander, Nature **420**, 297 (2002).
- [67] H. Hu, A. Cai, L. Chen, L. Deng, J. H. Pixley, K. Ingersent, and Q. Si (2021), *arXiv:2109.13224*.
- [68] M. B. Maple, E. D. Bauer, V. S. Zapf, and J. Wosnitzer, in *The Physics of Superconductors*, edited by K. H. Bennemann and J. B. Ketterson (Springer, Berlin, Heidelberg, 2004), vol. II, pp. 555–730.
- [69] C. Pfleiderer, Rev. Mod. Phys. **81**, 1551 (2009).
- [70] P. A. Lee, N. Nagaosa, and X.-G. Wen, Rev. Mod. Phys. **78**, 17 (2006).
- [71] K. Kanoda, in *The physics of organic superconductors and conductors*, edited by A. Lebed (Springer-Verlag, Berlin, Heidelberg, 2008), pp. 623–642.